Published in final edited form as:
J Immunol. 2010 September 1; 185(5): 2951–2959. doi:10.4049/jimmunol.1000732.

Distinctive CD3 Heterodimeric Ectodomain Topologies Maximize Antigen-Triggered Activation of αβ T Cell Receptors

Sun Taek Kim[*,†], **Maki Touma**[*,†], **Koh Takeuchi**[‡], **Zhen-Yu J. Sun**[‡], **Vibhuti P. Dave**[§], **Dietmar J. Kappes**[¶], **Gerhard Wagner**[‡], and **Ellis L. Reinherz**[*,†]

[*] Laboratory of Immunobiology and Department of Medical Oncology, Dana-Farber Cancer Institute, Harvard Medical School, Boston, MA 02115

[†] Department of Medicine, Harvard Medical School, Boston, MA 02115

[‡] Department of Biological Chemistry and Molecular Pharmacology, Harvard Medical School, Boston, MA 02115

[§] Lymphocyte Development Laboratory, Clinical Research Institute of Montreal, Montreal, Quebec, Canada

[¶] Blood Cell Development and Cancer Program, Fox Chase Cancer Center, Philadelphia, PA 19111

Abstract

The αβ TCR has recently been suggested to function as an anisotropic mechanosensor during immune surveillance, converting mechanical energy into a biochemical signal upon specific peptide/MHC ligation of the αβ clonotype. The heterodimeric CD3εγ and CD3εδ subunits, each composed of two Ig-like ectodomains, form unique side-to-side hydrophobic interfaces involving their paired G-strands, rigid connectors to their respective transmembrane segments. Those dimers are laterally disposed relative to the αβ heterodimer within the TCR complex. In this paper, using structure-guided mutational analysis, we investigate the functional consequences of a striking asymmetry in CD3γ and CD3δ G-strand geometries impacting ectodomain shape. The uniquely kinked conformation of the CD3γ G-strand is crucial for maximizing Ag-triggered TCR activation and surface TCR assembly/expression, offering a geometry to accommodate juxtaposition of CD3γ and TCR β ectodomains and foster quaternary change that cannot be replaced by the isologous CD3δ subunit's extracellular region. TCRβ and CD3 subunit protein sequence analyses among Gnathostomata species show that the Cβ FG loop and CD3γ subunit coevolved, consistent with this notion. Furthermore, restoration of T cell activation and development in CD3$\gamma^{-/-}$ mouse T lineage cells by interspecies replacement can be rationalized from structural insights on the topology of chimeric mouse/human CD3εδ dimers. Most importantly, our findings imply that CD3γ and CD3δ evolved from a common precursor gene to optimize peptide/MHC-triggered αβ TCR activation.

T cell receptors mediate Ag-specific recognition of peptides bound to MHC (pMHC) molecules via their Fab-like heterodimeric clonotypes. The TCR complex consists of αβ, CD3εγ, CD3εδ, and CD3ζζ dimers in a 1:1:1:1 stoichiometry. Whereas the function of the αβ clonotype is to bind pMHC, the associated CD3 subunits mediate signaling through their cytoplasmic (Cyt) tails (1–6). Assembly of the TCR complex is dependent on the transmembrane segment

Address correspondence and reprint requests to Dr. Ellis L. Reinherz at the current address: 77 Avenue Louis Pasteur, HIM 419, Boston, MA 02115. ellis_reinherz@dfci.harvard.edu.

The online version of this article contains supplemental material.

Disclosures
The authors have no financial conflicts of interest.

of the individual subunits and their unique disposition of charged residues in the hydrophobic membrane environment, as detailed elsewhere (7). The ectodomain of αβ and the Ig-like CD3εγ and CD3εδ heterodimers make a limited number of contacts with one another such that, in solution, no interactions are definable by nuclear magnetic resonance (NMR) (8,9). These results imply a loose association of individual dimeric extracellular TCR segments in the resting state.

How pMHC ligation of the αβ heterodimer on the T cell surface evokes intracellular signaling via the adjacent CD3 components has been the subject of intense investigation. Previous models suggest that TCRs transmit activation signals upon specific pMHC ligation via clustering, conformational changes, or combining both (1,10–14). Recently we proposed that a common TCR quaternary change rather than conformational alterations of αβ clonotypes by pMHCs facilitates signal initiation (15). Given the vast array of TCRs and their pMHC ligands, this appears to represent a practical solution to the T cell immune recognition problem. Clues regarding this mechanism were revealed from structural detailing of TCR complex components and by mAb binding studies and analysis of their effects on T cell function. For example, solution structures of CD3εγ and CD3εδ heterodimers reveal a unique side-to-side hydrophobic interface with conjoined β-sheets involving the G-strands of the two Ig-like ectodomains of each pair (8,9). The squat and rigid CD3 connecting segments contrast sharply with the long and flexible α and β connecting peptide linking respective constant domains to the transmembrane segments. These opposing features suggested that the αβ heterodimer may move relative to the CD3εγ and CD3εδ dimers upon pMHC ligation. By impeding such movement with H57, an Ab that bridges Cβ and CD3εγ (15,16), pMHC-triggered activation is blocked, consistent with this view.

Agonist anti-CD3 mAbs like 2C11 and 500A2 footprint to the membrane distal CD3ε lobe that they approach diagonally, adjacent to the lever-like Cβ FG loop that facilitates pMHC-triggered activation (17,18). This is the most sensitive TCR triggering direction (15). In contrast, a nonagonist mAb, 17A2, binds to the cleft between CD3ε and CD3γ in a perpendicular mode. 17A2 becomes stimulatory only subsequent to application of an external tangential (but not normal) force of ~50 pN introduced via optical tweezers. Specific pMHC, but not irrelevant pMHC, activates a T cell upon application of a similar force. During immune surveillance, when specific TCR-pMHC ligation occurs, an extracellular mechanical torque may be applied to the TCR prior to “stop movement” of the T cell. In this process, the pMHC on the APC functions as a gaff or hook to pull on the ligated TCR on the opposing T cell. Collectively, these findings suggest that the TCR is an anisotropic (i.e., directional) mechanosensor.

We reasoned that detailed analysis of the distinct topology of CD3 heterodimers would provide further insight into the basis of signal transduction involving the ectodomain components of the TCR mechanosensor. In addition, the rationale for differences in CD3 subunit requirements for various T lineage populations and developmental stages might emerge (19–28). In this study we have focused on differential G-strand geometry in CD3γ and CD3δ ectodomain fragments observed in human and other mammalian species. These features make the topology of CD3εγ and of CD3εδ distinct from one another and, in turn, mandate a defined quaternary organization for the TCR. The findings suggest that despite the loose confederacy of dimeric ectodomains constituting the TCR complex, dynamic complementarity of structural elements maximizes sensitivity in the relay of quaternary change essential for signal transduction.

Materials and Methods

Abs and flow cytometric analysis

The following fluorochrome-labeled mAbs were used for surface receptor analysis by flow cytometry: FITC–anti-CD3 (2C11), Alexa Fluor 647–anti-CD3 (17A2), Pacific Blue-CD4

(H129.19), Pacific Orange anti-CD8α (53-6.7), PE–anti-Vβ5 (MR9.4), and FITC-conjugated anti-TCR Cβ (H57) (BD Pharmingen, San Diego, CA). For flow cytometry, single-cell suspensions of thymocytes or lymph node (LN) cells were prepared at 5×10^6 cells/ml in PBS containing 2% FCS and 0.05% NaN_3. Those cells were triple- or five-color stained with the mAbs at saturating concentrations according to standard procedures. A FACScan or FACSAria (BD Biosciences, San Jose, CA) was used for flow cytometric measurements. Data analysis was performed using FlowJo software (Tree Star, Ashland, OR) after dead cells were excluded from the analysis by forward and side scatter gating.

Mice

C57BL/6 mice were purchased from Taconic Farms (Germantown, NY). CD3δ$^{-/-}$ mice and CD3γ$^{-/-}$ mice have been described in detail elsewhere (22,24). N15TCRtgCD3γ$^{-/-}$ mice were generated by crossing N15TCRtgRAG-2$^{-/-}$ (29) and CD3γ$^{-/-}$ mice. Construction of CD3δ mutant mice will be described in detail elsewhere (V.P. Dave and D.J. Kappes, unpublished observations). Mice were maintained and bred under specific pathogen-free conditions in the animal facility of the Dana-Farber Cancer Institute under a protocol reviewed and approved by the Animal Care and Use Committee. Mutant CD3δ cDNAs A–D (Fig. 2) were generated by PCR, confirmed by sequencing, and inserted into the human CD2 minigene cassette (30). Those transgenic (tg) lines were created by the Fox Chase Cancer Center Transgenic Facility (Philadelphia, PA) according to established protocols.

Mutagenesis of murine CD3γ

The cDNA encoding murine CD3γ was subcloned into the pUC18 for mutation and sequencing. To generate the CD3γ6M mutant in which the six amino acids in the G-strand of CD3γ (ETSNPL) were replaced with those of CD3δ (KVVSSV), we used the QuickChange Site-Directed Mutagenesis System (Stratagene, La Jolla, CA). CD3γmδ_{ecto} or CD3γhδ_{ecto} mutant was constructed by replacing the whole ectodomain denoted in Fig. 1 by recombinant PCR methods. CD3γ wild-type (wt) or CD3γ mutant constructs all contained a C-terminal FLAG epitope (DYKDDDDK) for quantitation of protein expression. All generated constructs were confirmed by DNA sequencing.

Retroviral transduction and peptide stimulation

For retroviral transduction, we used the pLZRS-IRES-eGFP vector encoding the enhanced GFP downstream of an internal ribosome entry site (31). The virus supernatant was prepared as described previously (17,32,33). For retroviral transduction with CD3γwt and mutant constructs, total LN cells from N15TCRtgCD3γ$^{-/-}$ mice were stimulated with 4 μg/ml concanavalin A for 2 d, and T cells were purified by removing I-A^b–positive cells using anti–I-A^b and magnetic beads. N15TCRtgCD3γ$^{-/-}$ T cells were placed in a 24-well plate at 10^6 cells/well (volume of 300 μl) in complete RPMI 1640 medium, and 300 μl viral supernatant containing 20 μg/ml Lipofectamin (Life Technologies-BRL, Carlsbad, CA) was added to each well and the plate centrifuged at 2000 rpm for 1 h at room temperature. Transduced T cells were cultured for 3 d with 50 μ/ml human rIL-2 until used for the assay. To assess the TCR signaling of transduced N15TCRtgCD3γ$^{-/-}$ T cells, cells were washed and stimulated with VSV8 peptide-loaded irradiated splenocytes from C57BL/6 mice or with plate-coated 2C11 (5 μg/ml) for 4 h in media containing GolgiPlug reagent (BD Pharmingen). Then, cells were stained for surface CD8 and for intracellular IFN-γ, using Fix/Perm solution (BD Pharmingen).

Fetal thymic organ culture with retroviral transduction

For retroviral transduction with CD3γwt and mutant constructs, fetal thymi were removed from day 14.5 CD3γ$^{-/-}$ fetuses (observation of vaginal plug is day 0.5), and thymocytes at 100,000 cells/well (volume of 100 μl) in fetal thymic organ culture (FTOC) medium supplemented with

50 ng/ml IL-7 and stem cell factor were placed in a 96-well plate. Next, 100 μl viral supernatant containing 20 μg/ml Lipofectamin (Life Technologies-BRL) was added to each well and the plate centrifuged at 2000 rpm for 1 h at room temperature, then incubated at 37°C overnight. The next day, cells were collected and 30 μl/well placed in a Terasaki plate. One fetal thymic lobe was placed in each well. The plate was inverted and incubated for 2 d. Thymic lobes from C57BL/6 were treated with 1.35 mM 2′-deoxyguanosine (Sigma-Aldrich, St. Louis, MO) in transwell inserts (Costar, Cambridge, MA) for 5 d before use to remove hematopoietic cells, but not epithelial tissue capable of allowing the differentiation of T cell precursors. After 2 d of hanging drop culture, lobes were transferred to ATTP 0.8 mM filters (Millipore, Billerica, MA) on Gelfoam (Pharmacia & Upjohn Company, Kalamazoo, MI). After 7 d, thymocytes were counted and analyzed by FACS. To determine transduction efficiency, 50,000 of the transduced cells were used for the FACS analysis of GFP expression.

Results

Structural comparison between CD3εγ and CD3εδ heterodimeric ectodomains

Solution structures of the murine CD3 (mCD3)εγ heterodimer and a chimeric CD3εδ heterodimer (mCD3ε and sheep CD3δ) reveal that both CD3ε domains adopt a virtually identical conformation with a root-mean-square-deviation <1.45 Å (8,9). Each heterodimer is composed of two Ig-like ectodomains with a hydrophobic interface brought together by hydrogen bond-paired terminal G-strands forming conjoined β-sheets. Unlike CD3ε, the CD3γ and CD3δ ectodomains within these heterodimers are more divergent from one another. In particular, structural comparison between CD3γ and CD3δ ectodomains shows that there is differential G-strand geometry resulting in a pronounced cleft between the two CD3 ectodomains in CD3εγ that is partially occluded in CD3εδ (Fig. 1*A*). The difference in G-strand disposition likely results from two factors. First, fewer hydrogen bonds are formed between the two G-strands in CD3εγ relative to those in CD3εδ, at least in part owing to an amino acid sequence of CD3γ that does not support the optimal packing between CD3ε and CD3γ at the N terminus (or top) of the G–G interaction surface. Second, relative to CD3γ, the CD3δ BC loop is five residues shorter, containing only four amino acids (Fig. 1*B*). The side view of the heterodimers in Fig. 1*A* (*right panel*) highlights the difference in CD3γ versus CD3δ FG and BC loops. The longer BC loop and the presence of the C′-strand force the entire GFCC' face of CD3γ, along with the FG loop, to bow away from the heterodimeric interface, whereas the shorter BC loop in CD3εδ must cut across the two β-sheets (ABED and FGCC′ faces), thereby preventing the FG loop from bending. The crystal structures of the human CD3 (hCD3)εγ and hCD3εδ heterodimers (Supplemental Fig. 1) identified a similar difference in G-strand geometry, as observed in the mouse orthologs (34,35). Note that the top of the hCD3εδ FG loop (Gly^{52}–Lys^{57}) is missing in the existing crystal structure coordinates, however, most likely owing to the inherent flexibility in this region of the human ortholog.

Differential G-strand geometries of CD3γ and CD3δ are recognized by the 17A2 anti-mCD3εγ mAb

Previous NMR binding experiments involving chemical shift and cross-saturation analyses (15) showed that 17A2 contacts both CD3ε and CD3γ domains, providing a structural explanation for preferential interaction of 17A2 with CD3εγ on the T cell surface. To investigate regions of CD3γ critical for native 17A2 binding, we used tg mice generated on the $CD3\delta^{-/-}$ background in which one of four segments of mCD3δ was replaced with a corresponding segment from mCD3γ (mutant [mut] A–D), as shown in Fig. 1*B*, and introduced into the mouse germline via transgenesis. The flow cytometric analysis in Fig. 2*A* reveals that both CD4 and CD8 T cells from $CD3\delta^{-/-}$ mice express low levels of residual 2C11-FITC (2C11-F) reactivity (mean fluorescence intensity [MFI] = 127 and 119, respectively; red curves), consistent with low-level CD3εγ surface expression in the absence of CD3εδ (24).

This 2C11-F staining is completely blocked by unlabeled 17A2 (MFI = 10–14; shaded blue curves). In contrast, the introduction of wtCD3δ on the CD3$\delta^{-/-}$ background restores 2C11-F reactivity (MFI = 1362–2060), and this binding is inhibited only by ~50% upon preincubation with unlabeled 17A2 (see also schematic in Fig. 2*A*, *right panel*). Similar patterns of reactivity and partial blockade of 2C11-F staining by unlabeled 17A2 preincubation are seen with introduction of mutA, mutB, and mutC CD3δ transgenes. However, mutD, involving substitution of the G-strand and a portion of the FG loop from CD3γ into CD3δ, results in T cells whose 2C11 binding is virtually completely blocked by 17A2 (Fig. 2*A*, mutD; shaded curve). The completeness of this 17A2-mediated inhibition of 2C11-F binding is comparable to that observed in the CD3$\delta^{-/-}$ T cells, indicating that 17A2 is able to bind to this mutant CD3εδ heterodimer (Fig. 2*A*, *right panel*). Further competitive binding experiments shown in Fig. 2*B* indicate that 17A2 inhibits 2C11 binding completely on αβ T cells from mutD mice, whereas in contrast, 17A2 inhibits 2C11 binding by only ~50% on αβ T cells from wt mice. Because murine γδ T cells lack CD3εδ, instead expressing two CD3εγ heterodimers per TCR complex (20), equivalent 2C11-F blocking activity by 17A2 on γδ T cells in both wt and mutD mice was expected and is observed (Fig. 2*B*).

Collectively, these findings show that the CD3γ G-strand segment is critical for 17A2 binding and that this segment can be introduced into CD3δ with no loss of TCR expression or function (Fig. 2). Such is not the case when residues in the CD3δ G-strand region are introduced into CD3γ (vide infra).

The CD3γ G-strand geometry is critical for TCR signaling

On the basis of the structural comparison and amino acid sequence alignment in Fig. 1, we generated a number of CD3γ mutants, including CD3γ6M, a variant in which the six amino acids in the G-strand of CD3γ (ETSNPL) at positions 70–75 were replaced with those of CD3δ (KVVSSV) (Fig. 1*A*). This swap is predicted to force the preceding segment and loop of the CD3γ6M mutant to adopt a more vertical trajectory than that of the CD3γwt counterpart. To test the functional significance of the CD3γ ectodomain modification, we exploited N15TCR tg mice specific for the vesicular stomatitis virus nuclear protein octapeptide (VSV8) bound to K^b (29,36) and bred onto a CD3$\gamma^{-/-}$ genetic background (22). Retroviral transduction of peripheral T cells from these animals with pLZRS-IRES-eGFP–containing CD3γwt or CD3γ mutant cDNAs encoding proteins schematically depicted in Fig. 3*A* gives rise to GFP-expressing transductants (GFP^+). As shown in Fig. 3*B*, CD3γwt retrovirally transduced N15tg CD3$\gamma^{-/-}$ T cells restores TCR surface expression, as monitored by flow cytometric analysis with each of four anti-TCR mAbs (MR 9.4, anti-Vβ5; 2C11, anti-CD3ε; H57, anti–TCR-Cβ; and 17A2, anti-CD3εγ). Note that this increase occurs only in the GFP^+ population (Fig. 3*B*). Although the CD3γ6M mutant restores much of the surface TCR expression (~60% of wtCD3γ), as assessed by MR9.4, 2C11, and H57 reactivity, 17A2 mAb binding to TCRs incorporating the CD3γ6M mutant is lost (Fig. 3*B*). These results support the notion that CD3γ6M adopts an extended G-strand more like mCD3δ, thereby preventing 17A2 mAb from binding in the cleft between CD3ε and CD3γ. Because the direct interaction residues mapped by proton-induced relaxation are exclusively in the CD3ε side (15), the trivial explanation that mutants abrogate 17A2 binding per se is excluded. Subsequently, we shortened the BC loop (LTDKT) in CD3γ by deleting the LTDKT sequence to create a second mutant, CD3γ6M-ΔBC. This foreshortened BC loop likely reinforces the upward trajectory of the FG loop in the CD3γ6M-ΔBC variant. Strikingly, the surface TCR expression rescue observed with CD3γ6M was not detected by any of the four Abs tested after CD3γ6M-ΔBC transduction. Collectively, these data suggest that this kinked CD3γ G-strand geometry is important for TCR surface expression, permitting CD3εγ to occupy a position beneath the Cβ FG loop of the β subunit and consistent with our previous TCR quaternary model (15) (Supplemental Fig. 2). In further support of this hypothesis, a third mutant in which the entire CD3γ ectodomain is replaced with

that of CD3δ (CD3γmδ$_{ecto}$) also fails to reconstitute TCR surface expression. Cellular protein expression for each of the mutant CD3γ transductants was comparable to that of wtCD3γ, as assessed by intracellular staining using the FLAG-tag appended to the Cyt tail of each construct and anti-FLAG Ab (Supplemental Fig. 3). However, we cannot exclude that in the case of CD3γ6M-ΔBC, incorrect protein folding may contribute to absent surface expression.

Next, following retroviral transduction, N15 T cells were stimulated with VSV8-pulsed K^b-expressing APCs. As shown by the representative experiment in Fig. 3*C*, no significant IFN-γ production was obtained from GFP$^+$ empty vector control transductants, whereas N15 T cells transduced with wtCD3γ cDNA showed specific responsiveness to VSV8 peptide in a concentration-dependent manner. N15 T cells expressing the CD3γ6M cDNA induced less IFN-γ production compared with that of CD3γwt, emphasizing the importance of the unique CD3γ G-strand geometry for Ag-triggered activation. As expected, VSV8 stimulation failed to induce IFN-γ production in N15 T cells transduced with CD3γ6M-ΔBC or CD3γmδ$_{ecto}$.

Fig. 3*D* represents a composite histogram of IFN-γ production from multiple experiments using VSV8 stimulation of retrovirally transduced N15tgCD3γ$^{-/-}$ T cells. Both CD3γwt and CD3γ6M transductants (GFP$^+$) produce IFN-γ upon VSV stimulation, but with cytokine production from CD3γwt greater than that from CD3γ6M transductants. Note the lack of detectable activation by pMHC in GFP$^-$ cells in either set of cultures. In contrast, with anti-CD3ε mAb triggering, IFN-γ production is observed in transduced (GFP$^+$) and nontransduced (GFP$^-$) populations, implying that 2C11 stimulation via CD3εδ induces detectable IFN-γ production. Nonetheless, transduction of CD3γwt significantly augments that 2C11-stimulated response, compared with the vector control. Similar 2C11-stimulated IFN-γ production in CD3γwt and CD3γ6M transductants suggests that differential responsiveness to pMHC is not a consequence of TCR expression level. Together, the findings imply that TCRβ-CD3εγ juxtaposition involving the kinked CD3γ G-strand affords an optimized geometry for effective Ag-triggered T cell activation.

Coevolution of the elongated Cβ FG loop and duplication of CD3γ plus CD3δ genes from a single precursor

Whereas the striking elongation of the Cβ FG loop among mammalian species is well conserved, sequence comparison with nonmammalian vertebrate species (chicken, fish, and frog) reveals that the lengthy Cβ FG loop is not observed in the latter (Fig. 4*A*). This rigid Cβ FG loop in mouse has been shown to facilitate both selection of thymocytes and activation of T cells (17,18). The absence of distinct CD3γ and CD3δ subunits in the above-mentioned nonmammalian species and expression of a single precursor CD3γ/δ gene have been shown based on genomic and biochemical analyses, as well as theoretical predictions dating the required CD3 duplication event (37–39). Although recently it has been demonstrated that the jawless vertebrates (agnathans) have alternative adaptive immune systems with variable lymphocyte receptors, all jawed vertebrates (gnathostomates) possess fully developed adaptive immune systems with TCR and Ig genes (40). Both the elongated Cβ FG loop and the distinct CD3γ and CD3δ genes are unique in the mammalian species among Gnathostamata (Fig. 4*B*). These analyses support the notion that TCRCβ and CD3γ have been evolutionarily coupled for TCR assembly and signaling in the mammalian species. Furthermore, these findings imply that the distinct topology of CD3 heterodimers coevolved with TCRC domains to optimize the quaternary TCR structure for pMHC-triggered αβ TCR activation. TCRαβ heterodimer assembly studies with various CD3 complexes, using a phylogenetic approach with TCR complex subunits from mammalian and nonmammalian vertebrates, support this conclusion (41).

Restoration of T cell signaling and development by heterologous replacement of the mCD3γ ectodomain

Despite the above results and conclusions, it has been reported that hCD3δ can partially restore thymic development in the absence of mCD3γ in CD3γ$^{-/-}$ mice (42,43), suggesting that the hCD3δ ectodomain may be accommodated in juxtaposition to the murine β subunit. We therefore assessed whether a chimeric CD3γ protein containing the hCD3δ ectodomain fused with transmembrane and Cyt tail segments of mCD3γ (CD3γhδ$_{ecto}$) could restore TCR surface expression and T cell activation in N15tgCD3γ$^{-/-}$ T cells. In contrast to the inability of CD3γmδ$_{ecto}$ chimera to restore TCR expression and function, CD3γhδ$_{ecto}$ was competent to do both. As shown in Fig. 5*A*, CD3γhδ$_{ecto}$ transduction induced surface TCR expression comparable to that of CD3γwt, although, not surprisingly, with loss of 17A2 mAb reactivity. In vitro stimulation experiments likewise showed that CD3γhδ$_{ecto}$ possesses a signaling capacity equivalent to that of CD3γwt to induce IFN-γ production upon pMHC- (Fig. 5*B*) or 2C11- mediated stimulation (Fig. 5*C*). Thus, CD3γhδ$_{ecto}$ serves as a suitable structural surrogate for both VSV8- and 2C11-triggered activation.

To next assess whether this CD3γhδ$_{ecto}$ chimera can provide differentiation signals during development, an FTOC system was employed. Thymocyte progenitors from CD3γ$^{-/-}$ fetal mice were transduced with CD3γwt or CD3γhδ$_{ecto}$ cDNA containing retroviruses of comparable viral titer. Subsequently, thymocytes generated within the reconstituted FTOC after 7 d of culture were prepared and analyzed for GFP expression and surface phenotype. As shown by CD4 and CD8 surface expression patterns in Fig. 5*D* (*top*), thymic development in the CD3γhδ$_{ecto}$ transduced thymocytes was equivalent or better than that of CD3γwt transduced thymocytes. In contrast to nontransduced cells (GFP^{-}) within the same FTOC cultures, the number of double positive thymocytes was increased 2- to 5-fold. Fig. 5*D* (*middle*) shows that double negative (DN) cell development from DN1 (CD44^{+}CD25^{-}) plus DN2 (CD44^{+}CD25^{+}) stages to DN3 (CD44^{-}CD25^{+}) and DN4 (CD44^{-}CD25^{-}) stages was also accelerated by the transduction of CD3γhδ$_{ecto}$. Thus, for example, in CD3γhδ$_{ecto}$ transductants, DN3 = 9.8% and DN4 = 42.2%, compared with 1.1 and 3.9%, respectively, for the GFP^{-} control. Furthermore, surface TCRβ expression on DN3/4 stage cells was only slightly higher than on nontransduced cells (Fig. 5*D*, *bottom*), suggesting that pre-TCR expression is supported by CD3γhδ$_{ecto}$, as it is with wtCD3γ without nonphysiological overexpression of the pre-TCR. These results imply that the CD3γhδ$_{ecto}$ protein can replace that of the wtCD3γ component in the pre-TCR during T cell development.

Our findings with the chimeric CD3γhδ$_{ecto}$ protein are in agreement with results generated through transgenesis in CD3γ$^{-/-}$ mice using the hCD3δ (human only) construct (42,43). Why, then, might these mouse-human interspecies CD3εδ heterodimers function to foster signaling (Fig. 6)? In this regard, it is noteworthy that the aromatic ring of Phe^{89} in human CD3ε makes hydrophobic interactions with both the γ-methyl of Thr^{62} and the hydrophobic β-methylene position of the Gln64 side chain of human CD3δ. This interaction creates a tightly packed interface between hCD3ε and hCD3δ molecules at the top of the G–G-strand interface (Supplemental Fig. 4). This preferential interaction would not be formed in the mCD3εγhδ$_{ecto}$ dimer, as the Phe^{89} in hCD3ε is a Thr in the corresponding position mCD3ε. As a result, the top of the G-strand in CD3γhδ$_{ecto}$ and hCD3δ proteins, when dimerized with mCD3ε, can bend and slot into the area normally accommodating mCD3εγ in the TCRβ–CD3εγ junction, without steric clash. Furthermore, hCD3δ contains four alternating charged residues at the end of the FG loop (K57/D58/K59/E60). This charge cluster would destabilize a straight-up β-strand conformation with two positively charged lysines on one side and two negatively charged residues on the back side. Thus, the FG loop of hCD3δ is most likely unstructured, consistent with its crystal structure (Supplemental Fig. 1) (35), and could be readily bent toward the back ABED face when heterodimerized with mCD3ε in a fashion

analogous to that of mCD3γ. Differential glycosylation of mCD3δ versus hCD3δ with one fewer *N*-linked adduct in the human ortholog may also contribute to the functionality of this replacement.

Discussion

Analysis of CD3 sequence divergence indicates that CD3γ, CD3δ, and CD3ε genes arose from a common ancestor in a two-step process of gene duplication (38). Mammals have three CD3 genes (γ, δ, and ε), whereas nonmammalians (birds, fish, and amphibians) have only two: a CD3γδ precursor and a CD3ε gene. Protein sequence comparison indicates that each CD3γ and CD3δ subunit evolved with highly homologous heterodimeric interfaces and membrane proximal segments for efficient and specific signaling transfer when paired with CD3ε. The compact orientation of the CD3γ FG loop and single horizontally attached glycan in the mouse is a feature of the CD3εγ heterodimer that affords lateral support of the C region domains for αβ as well as γδ TCRs. In addition, CD3εγ appears to have adapted to optimally interact with the Cβ FG loop. Our findings that the elongation of the structured Cβ FG loop coevolved with appearance of the CD3γ gene from a CD3γ/δ precursor are strong support for this notion. By contrast, the more vertical CD3δ FG loop trajectory and greater number of *N*-linked glycan adducts in CD3εδ heterodimers assume a more extended geometry that cannot fit into the homologous TCRβ–CD3εγ interaction site (15). The CD3εδ disposition on the TCRα "side" of the complex occupies intervening space between the coreceptor (CD4 or CD8) and the αβ heterodimer (44,45). This bulky CD3εδ component may also be entropically advantageous to help preconfigure the coreceptor as a TCR, pMHC, and coreceptor ternary complex forms.

The crystal structure of a γδ TCR heterodimer reveals a Cγ–Cδ domain symmetry, in contradistinction to the Cα–Cβ domain asymmetry observed in αβ TCRs (16,46,47). The γδ TCR heterodimer also differs by lacking an elongated Cβ FG loop equivalent. γδ TCR lineage commitment is associated with more robust signaling relative to that of the αβ TCR, with greater TCR copy number and/or ligand density likely affecting γδ T lineage signaling strength (22, 48). In contrast, αβ TCR pMHC ligands are present at low levels, mandating additional TCR modifications to compensate for weak signals promoting αβ T cell fate and function. During immune surveillance, continued cell movement following ligation of the TCR αβ clonotype by specific pMHC fosters quaternary change; the Cβ FG loop interacts with CD3εγ on one side of the TCR and the Cα domain with the bulky CD3εδ heterodimer on the other. It is the tangential rather than normal (i.e., perpendicular to the membrane) directional force that triggers TCR activation post-pMHC ligation, as shown by optical tweezer experiments (15).

Our current results emphasize how the αβ TCR quaternary structure is optimal for surface expression and signaling. Fig. 6*A* gives a side view of the surface-exposed TCR complex based upon existing structural information of individual components and molecular modeling (8, 15,49). The substantial *N*-linked glycosylation of TCR subunits is indicated by the brown space-filling molecular representations. On the TCRβ "side," the Cβ FG loop (17,18) and the compact orientation of the CD3γ FG loop (Fig. 1,Supplemental Fig. 2) are key features contributing to the asymmetry optimizing TCR signaling. Lateral movement of the TCRαβ heterodimer can apply a torque on CD3εγ via the Cβ FG loop appendage. Fig. 6*B* schematically demonstrates that the extended CD3δ subunit ectodomain would sterically clash with the Cβ FG loop above, whereas that of CD3γ or the chimeric heterodimer does not. On the TCRα "side," the bulky glycans and vertical CD3δ FG loop disposition may also likewise relay quaternary change to CD3εδ after tangential force-induced torque. Alternatively, the torque on CD3εδ could be applied through the highly conserved connecting peptide at the base of the TCRCα domain (30). Further studies aimed at rigidifying or derigidifying segments of the TCR complex, without altering pMHC binding, should show an impact on TCR signaling, consistent with a mechanosensor mechanism of action.

The ability of the hCD3δ ectodomain to pair with mCD3ε and foster TCR complex expression signaling, as well as murine thymocyte development, might appear, at first glance, contradictory to our view that CD3γ and CD3δ ectodomains evolved to occupy a different side of the TCR complex. However, that is not the case. Isologous subunit ectodomain substitution is not permitted, whereas the heterologous hCD3δ ectodomain can replace that of mCD3γ. That functional substitution, as noted in Supplemental Fig. 4, is possible because mCD3ε has a Thr residue in lieu of Phe89 in hCD3ε, allowing the top of the G-strand of hCD3δ, when paired with mCD3ε, to avoid steric clash with the TCRβ subunit. We emphasize that the geometry of mCD3γ and mCD3δ G-strand N-terminal residues (residues 70–75 and residues 58–63) are distinct from each other, as are the corresponding segments in the respective human orthologs.

As structural and functional analyses of these and other Ig-like domains of receptors become more sophisticated, additional subtleties and their biological implications will be revealed. The details as described in this study for CD3 heterodimers demonstrate the important functional consequences of structural evolution. Understanding these differences will help with elucidating the function of multisubunit receptors, such as the TCR.

Supplementary Material

Refer to Web version on PubMed Central for supplementary material.

Acknowledgments

We thank Haesook Kim for statistical analysis, Maris Handley for flow cytometry, and Jiahuai Wang for careful review of this manuscript.

This work was supported by National Institutes of Health Grants AI19807 (to E.L.R.), CA74620 (to D.J.K.), AI37581, GM47467, and EB002026 (to G.W.), and Canadian Institutes of Health Research Grant 81145 (to V.P.D.).

Abbreviations in this paper

17A2-A647	17A2-Alexa Fluor 647
2C11-F	2C11-FITC
Cyt	cytoplasmic
DN	double negative
FTOC	fetal thymic organ culture
hCD3	human CD3
LN	lymph node
mCD3	murine CD3
MFI	mean fluorescence intensity
mut	mutant
NMR	nuclear magnetic resonance
pMHC	peptide bound to MHC
tg	transgenic
TM	transmembrane
wt	wild-type

References

1. Smith-Garvin JE, Koretzky GA, Jordan MS. T cell activation. Annu Rev Immunol 2009;27:591–619. [PubMed: 19132916]
2. Rudolph MG, Stanfield RL, Wilson IA. How TCRs bind MHCs, peptides, and coreceptors. Annu Rev Immunol 2006;24:419–466. [PubMed: 16551255]
3. Romeo C, Amiot M, Seed B. Sequence requirements for induction of cytolysis by the T cell antigen/Fc receptor zeta chain. Cell 1992;68:889–897. [PubMed: 1547489]
4. Letourneur F, Klausner RD. Activation of T cells by a tyrosine kinase activation domain in the cytoplasmic tail of CD3 epsilon. Science 1992;255:79–82. [PubMed: 1532456]
5. Irving BA, Weiss A. The cytoplasmic domain of the T cell receptor zeta chain is sufficient to couple to receptor-associated signal transduction pathways. Cell 1991;64:891–901. [PubMed: 1705867]
6. Reth M. Antigen receptor tail clue. Nature 1989;338:383–384. [PubMed: 2927501]
7. Call ME, Wucherpfennig KW. Common themes in the assembly and architecture of activating immune receptors. Nat Rev Immunol 2007;7:841–850. [PubMed: 17960150]
8. Sun ZY, Kim ST, Kim IC, Fahmy A, Reinherz EL, Wagner G. Solution structure of the CD3epsilondelta ectodomain and comparison with CD3epsilongamma as a basis for modeling T cell receptor topology and signaling. Proc Natl Acad Sci USA 2004;101:16867–16872. [PubMed: 15557001]
9. Sun ZJ, Kim KS, Wagner G, Reinherz EL. Mechanisms contributing to T cell receptor signaling and assembly revealed by the solution structure of an ectodomain fragment of the CD3 epsilon gamma heterodimer. Cell 2001;105:913–923. [PubMed: 11439187]
10. Beddoe T, Chen Z, Clements CS, Ely LK, Bushell SR, Vivian JP, Kjer-Nielsen L, Pang SS, Dunstone MA, Liu YC, et al. Antigen ligation triggers a conformational change within the constant domain of the alphabeta T cell receptor. Immunity 2009;30:777–788. [PubMed: 19464197]
11. Ma Z, Sharp KA, Janmey PA, Finkel TH. Surface-anchored monomeric agonist pMHCs alone trigger TCR with high sensitivity. PLoS Biol 2008;6:e43. [PubMed: 18303949]
12. Minguet S, Swamy M, Alarcón B, Luescher IF, Schamel WW. Full activation of the T cell receptor requires both clustering and conformational changes at CD3. Immunity 2007;26:43–54. [PubMed: 17188005]
13. Alarcón B, Swamy M, van Santen HM, Schamel WW. T-cell antigen-receptor stoichiometry: pre-clustering for sensitivity. EMBO Rep 2006;7:490–495. [PubMed: 16670682]
14. Choudhuri K, Wiseman D, Brown MH, Gould K, van der Merwe PA. T-cell receptor triggering is critically dependent on the dimensions of its peptide-MHC ligand. Nature 2005;436:578–582. [PubMed: 16049493]
15. Kim ST, Takeuchi K, Sun ZY, Touma M, Castro CE, Fahmy A, Lang MJ, Wagner G, Reinherz EL. The alphabeta T cell receptor is an anisotropic mechanosensor. J Biol Chem 2009;284:31028–31037. [PubMed: 19755427]
16. Wang J, Lim K, Smolyar A, Teng M, Liu J, Tse AG, Liu J, Hussey RE, Chishti Y, Thomson CT, et al. Atomic structure of an alphabeta T cell receptor (TCR) heterodimer in complex with an anti-TCR fab fragment derived from a mitogenic antibody. EMBO J 1998;17:10–26. [PubMed: 9427737]
17. Touma M, Chang HC, Sasada T, Handley M, Clayton LK, Reinherz EL. The TCR C beta FG loop regulates alpha beta T cell development. J Immunol 2006;176:6812–6823. [PubMed: 16709841]
18. Sasada T, Touma M, Chang HC, Clayton LK, Wang JH, Reinherz EL. Involvement of the TCR Cbeta FG loop in thymic selection and T cell function. J Exp Med 2002;195:1419–1431. [PubMed: 12045240]
19. Hayes SM, Shores EW, Love PE. An architectural perspective on signaling by the pre-, alphabeta and gammadelta T cell receptors. Immunol Rev 2003;191:28–37. [PubMed: 12614349]
20. Hayes SM, Love PE. Distinct structure and signaling potential of the gamma delta TCR complex. Immunity 2002;16:827–838. [PubMed: 12121664]
21. Wang B, Wang N, Salio M, Sharpe A, Allen D, She J, Terhorst C. Essential and partially overlapping role of CD3gamma and CD3delta for development of alphabeta and gammadelta T lymphocytes. J Exp Med 1998;188:1375–1380. [PubMed: 9763617]

22. Haks MC, Krimpenfort P, Borst J, Kruisbeek AM. The CD3gamma chain is essential for development of both the TCRalphabeta and TCRgammadelta lineages. EMBO J 1998;17:1871–1882. [PubMed: 9524111]
23. DeJarnette JB, Sommers CL, Huang K, Woodside KJ, Emmons R, Katz K, Shores EW, Love PE. Specific requirement for CD3epsilon in T cell development. Proc Natl Acad Sci USA 1998;95:14909–14914. [PubMed: 9843989]
24. Dave VP, Cao Z, Browne C, Alarcon B, Fernandez-Miguel G, Lafaille J, de la Hera A, Tonegawa S, Kappes DJ. CD3 delta deficiency arrests development of the alpha beta but not the gamma delta T cell lineage. EMBO J 1997;16:1360–1370. [PubMed: 9135151]
25. Malissen M, Gillet A, Ardouin L, Bouvier G, Trucy J, Ferrier P, Vivier E, Malissen B. Altered T cell development in mice with a targeted mutation of the CD3-epsilon gene. EMBO J 1995;14:4641–4653. [PubMed: 7588594]
26. Malissen M, Gillet A, Rocha B, Trucy J, Vivier E, Boyer C, Köntgen F, Brun N, Mazza G, Spanopoulou E, et al. T cell development in mice lacking the CD3-zeta/eta gene. EMBO J 1993;12:4347–4355. [PubMed: 8223444]
27. Love PE, Shores EW, Johnson MD, Tremblay ML, Lee EJ, Grinberg A, Huang SP, Singer A, Westphal H. T cell development in mice that lack the zeta chain of the T cell antigen receptor complex. Science 1993;261:918–921. [PubMed: 7688481]
28. Liu CP, Ueda R, She J, Sancho J, Wang B, Weddell G, Loring J, Kurahara C, Dudley EC, Hayday A, et al. Abnormal T cell development in CD3-zeta$^{-/-}$ mutant mice and identification of a novel T cell population in the intestine. EMBO J 1993;12:4863–4875. [PubMed: 8223495]
29. Ghendler Y, Teng MK, Liu JH, Witte T, Liu J, Kim KS, Kern P, Chang HC, Wang JH, Reinherz EL. Differential thymic selection outcomes stimulated by focal structural alteration in peptide/major histocompatibility complex ligands. Proc Natl Acad Sci USA 1998;95:10061–10066. [PubMed: 9707600]
30. Bäckström BT, Müller U, Hausmann B, Palmer E. Positive selection through a motif in the alphabeta T cell receptor. Science 1998;281:835–838. [PubMed: 9694657]
31. Jaleco AC, Stegmann AP, Heemskerk MH, Couwenberg F, Bakker AQ, Weijer K, Spits H. Genetic modification of human B-cell development: B-cell development is inhibited by the dominant negative helix loop helix factor Id3. Blood 1999;94:2637–2646. [PubMed: 10515867]
32. Touma M, Sun ZY, Clayton LK, Marissen WE, Kruisbeek AM, Wagner G, Reinherz EL. Importance of the CD3gamma ectodomain terminal beta-strand and membrane proximal stalk in thymic development and receptor assembly. J Immunol 2007;178:3668–3679. [PubMed: 17339464]
33. Kinsella TM, Nolan GP. Episomal vectors rapidly and stably produce high-titer recombinant retrovirus. Hum Gene Ther 1996;7:1405–1413. [PubMed: 8844199]
34. Kjer-Nielsen L, Dunstone MA, Kostenko L, Ely LK, Beddoe T, Mifsud NA, Purcell AW, Brooks AG, McCluskey J, Rossjohn J. Crystal structure of the human T cell receptor CD3 epsilon gamma heterodimer complexed to the therapeutic mAb OKT3. Proc Natl Acad Sci USA 2004;101:7675–7680. [PubMed: 15136729]
35. Arnett KL, Harrison SC, Wiley DC. Crystal structure of a human CD3-epsilon/delta dimer in complex with a UCHT1 single-chain antibody fragment. Proc Natl Acad Sci USA 2004;101:16268–16273. [PubMed: 15534202]
36. Shibata K, Imarai M, van Bleek GM, Joyce S, Nathenson SG. Vesicular stomatitis virus antigenic octapeptide N52-59 is anchored into the groove of the H-2Kb molecule by the side chains of three amino acids and the main-chain atoms of the amino terminus. Proc Natl Acad Sci USA 1992;89:3135–3139. [PubMed: 1313583]
37. Göbel TW, Meier EL, Du Pasquier L. Biochemical analysis of the *Xenopus laevis* TCR/CD3 complex supports the “stepwise evolution” model. Eur J Immunol 2000;30:2775–2781. [PubMed: 11069057]
38. Göbel TW, Dangy JP. Evidence for a stepwise evolution of the CD3 family. J Immunol 2000;164:879–883. [PubMed: 10623835]
39. Krissansen GW, Owen MJ, Fink PJ, Crumpton MJ. Molecular cloning of the cDNA encoding the T3 gamma subunit of the mouse T3/T cell antigen receptor complex. J Immunol 1987;138:3513–3518. [PubMed: 2952720]

40. Cooper MD, Alder MN. The evolution of adaptive immune systems. Cell 2006;124:815–822. [PubMed: 16497590]
41. Gouaillard C, Huchenq-Champagne A, Arnaud J, Chen CL, Rubin B. Evolution of T cell receptor (TCR) alpha beta heterodimer assembly with the CD3 complex. Eur J Immunol 2001;31:3798–3805. [PubMed: 11745401]
42. Pan Q, Brodeur JF, Drbal K, Dave VP. Different role for mouse and human CD3delta/epsilon heterodimer in preT cell receptor (preTCR) function: human CD3delta/epsilon heterodimer restores the defective preTCR function in CD3gamma- and CD3gammadelta-deficient mice. Mol Immunol 2006;43:1741–1750. [PubMed: 16412509]
43. Fernández-Malavé E, Wang N, Pulgar M, Schamel WW, Alarcón B, Terhorst C. Overlapping functions of human CD3delta and mouse CD3gamma in alphabeta T-cell development revealed in a humanized CD3gamma-mouse. Blood 2006;108:3420–3427. [PubMed: 16888097]
44. Wang JH, Meijers R, Xiong Y, Liu JH, Sakihama T, Zhang R, Joachimiak A, Reinherz EL. Crystal structure of the human CD4 N-terminal two-domain fragment complexed to a class II MHC molecule. Proc Natl Acad Sci USA 2001;98:10799–10804. [PubMed: 11535811]
45. Moody AM, Xiong Y, Chang HC, Reinherz EL. The CD8alphabeta co-receptor on double-positive thymocytes binds with differing affinities to the products of distinct class I MHC loci. Eur J Immunol 2001;31:2791–2799. [PubMed: 11536178]
46. Adams EJ, Chien YH, Garcia KC. Structure of a gammadelta T cell receptor in complex with the nonclassical MHC T22. Science 2005;308:227–231. [PubMed: 15821084]
47. Garboczi DN, Ghosh P, Utz U, Fan QR, Biddison WE, Wiley DC. Structure of the complex between human T-cell receptor, viral peptide and HLA-A2. Nature 1996;384:134–141. [PubMed: 8906788]
48. Hayes SM, Li L, Love PE. TCR signal strength influences alphabeta/gammadelta lineage fate. Immunity 2005;22:583–593. [PubMed: 15894276]
49. Wyss DF, Choi JS, Li J, Knoppers MH, Willis KJ, Arulanandam AR, Smolyar A, Reinherz EL, Wagner G. Conformation and function of the N-linked glycan in the adhesion domain of human CD2. Science 1995;269:1273–1278. [PubMed: 7544493]

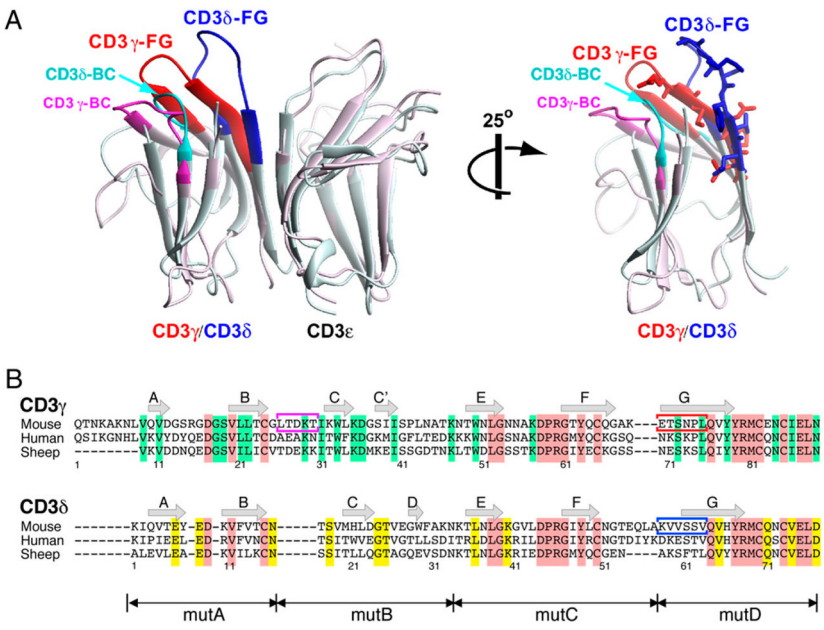

FIGURE 1.

Structural comparison between mCD3εγ and mCD3εδ heterodimers. *A*, Ribbon diagram showing heterodimeric CD3εγ and CD3εδ structures superimposed on CD3ε. NMR structures of CD3εγ (Protein Data Bank code: 1JBJ) and CD3εδ (Protein Data Bank code: 1XMW) were used for structural comparison. We compared the lowest energy structure from the ensemble of NMR structures. CD3εγ and CD3εδ are shown in pink and light blue, respectively. Structural differences are highlighted in G-strands, FG loops, and BC loops, as denoted. Another view representing a rotation about the vertical pseudo 2-fold axis (*right panel*) highlights differences in G-strand geometry between CD3γ and CD3δ. The key residues (70–75) for unique G-strand geometry in both CD3γ and CD3δ are shown as stick models. For clarity, the peptide linkers are not shown in the figure. *B*, Amino acid sequence alignments of CD3γ and CD3δ from mouse, human, and sheep. The residues conserved among all CD3γ and CD3δ orthologs are shown in red background. The residues conserved among CD3γ or CD3δ sequences are shown in green or yellow background, respectively. The β-strands depicted above the sequences are taken from mCD3γ and sheep CD3δ NMR structures. For each mutA–D shown in Fig. 2, the denoted amino acid sequence of the mCD3δ fragment replaced with the corresponding mCD3γ fragment is delineated. Mutation sites for the G-strand and BC loop in CD3γ are denoted by red and purple brackets, respectively. The corresponding G-strand region in CD3δ used for replacement is denoted by blue brackets.

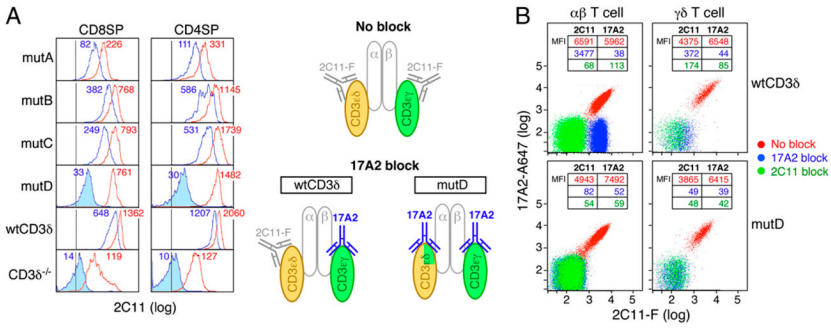

FIGURE 2.

Introduction of the CD3γ G-strand into CD3δ creates an mCD3εγ chimera reactive with 17A2. *A*, Binding of 17A2 and 2C11 to αβ T cells of wt, CD3δ$^{-/-}$, and CD3δ mutant mice. For each CD3δ mutA–D, a denoted amino acid segment of mCD3δ was replaced by the corresponding mCD3γ fragment (Fig. 1*B*). Peripheral lymphocytes from mutA, mutB, mutC, mutD, wtCD3δ, and CD3δ$^{-/-}$ mice were examined by flow cytometry. 2C11-F staining was determined with or without prior unlabeled 17A2 blockade (100 μg/ml). The red line represents 2C11-F staining without blockade, whereas the blue line represents 2C11-F staining after 17A2 blockade. Numbers denote MFI. The curves shaded blue show similarity in 17A2 blockade, reducing 2C11-F to essentially background staining levels. 2C11-F binding on αβ T cells with or without prior unlabeled17A2 blockade is depicted schematically. *B*, Binding competition between 17A2 and 2C11 on the T cell surface from wtCD3δ and mutD mice. LNs were isolated and stained with mAbs against T cell surface markers for flow cytometric analysis. Each dot represents 2C11-F and 17A2-Alexa Fluor 647 binding after unlabeled 17A2 blocking (blue), 2C11 blocking (green), or no preincubation (red). αβ TCR^{+} (CD4SP^{+}) or γδ TCR^{+} populations were gated for analysis. Data are representative of three experiments. 17A2-A647, 17A2-Alexa Fluor 647.

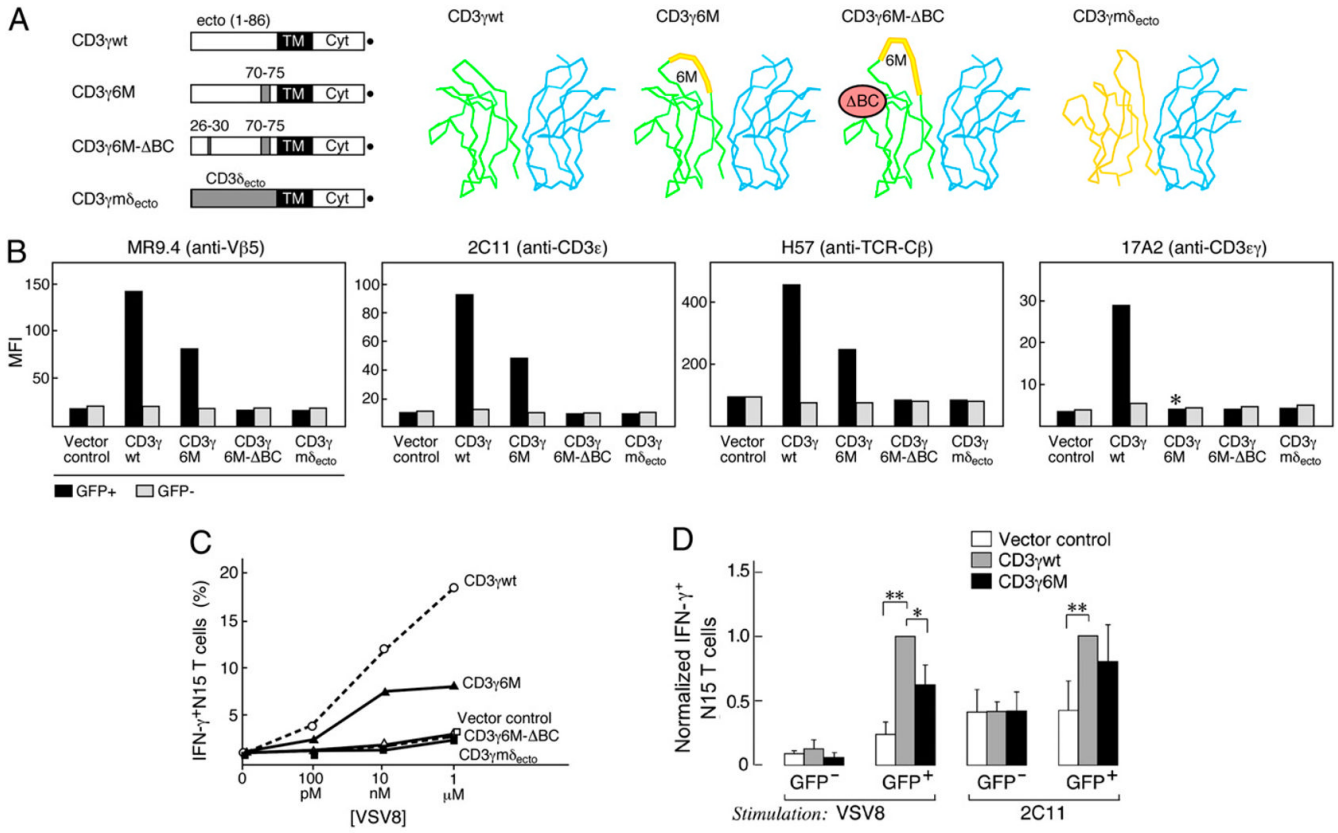

FIGURE 3.

The unique G-strand geometry of CD3γ is important for TCR complex surface expression and signaling. *A*, Schematic drawing of mCD3γwt and CD3γ ectodomain mutant constructs. All constructs contain transmembrane and Cyt domains of mCD3γ, as well as a C-terminal FLAG-tag (●). The mutation positions in CD3γ ectodomain are denoted in the accompanying ribbon diagrams (CD3ε, cyan; CD3γ, green; and CD3δ, yellow). *B*, Surface TCR expression on N15TCRtgCD3$\gamma^{-/-}$ T cells after CD3γwt and CD3γ ectodomain mutant transduction. N15 T cells were stained with each indicated mAb and analyzed by flow cytometry after retroviral transduction. Data are representative of three independent experiments. *C*, pMHC/TCR-mediated signaling in N15TCRtgCD3$\gamma^{-/-}$ T cell transfectants. Transduced N15 T cells were stimulated with VSV8 peptide-loaded APCs for 4 h. The number of cytokine-producing cells was measured using flow cytometry after gating each GFP$^+$CD8$^+$ population in one representative experiment. *D*, Statistical analysis of VSV8- or 2C11-stimulated N15TCRtgCD3$\gamma^{-/-}$ transduced populations. Transduced T cells were stimulated by VSV8 peptide (1 μM) or plate-bound 2C11 Ab (5 μg/ml). GFP$^-$CD8$^+$ and GFP$^+$CD8$^+$ populations were gated for IFN-γ$^+$ analysis. The number of cytokine-producing cells was normalized by setting the IFN-γ amount from the CD3γwt transduced N15TCRtgCD3$\gamma^{-/-}$ T cells as 1 and no stimulation as 0. Two-sided exact Wilcoxon rank-sum test was used to compare. Values are average ± SD (n = 3). *$p \leq 0.05$; **$p \leq 0.01$. TM, transmembrane.

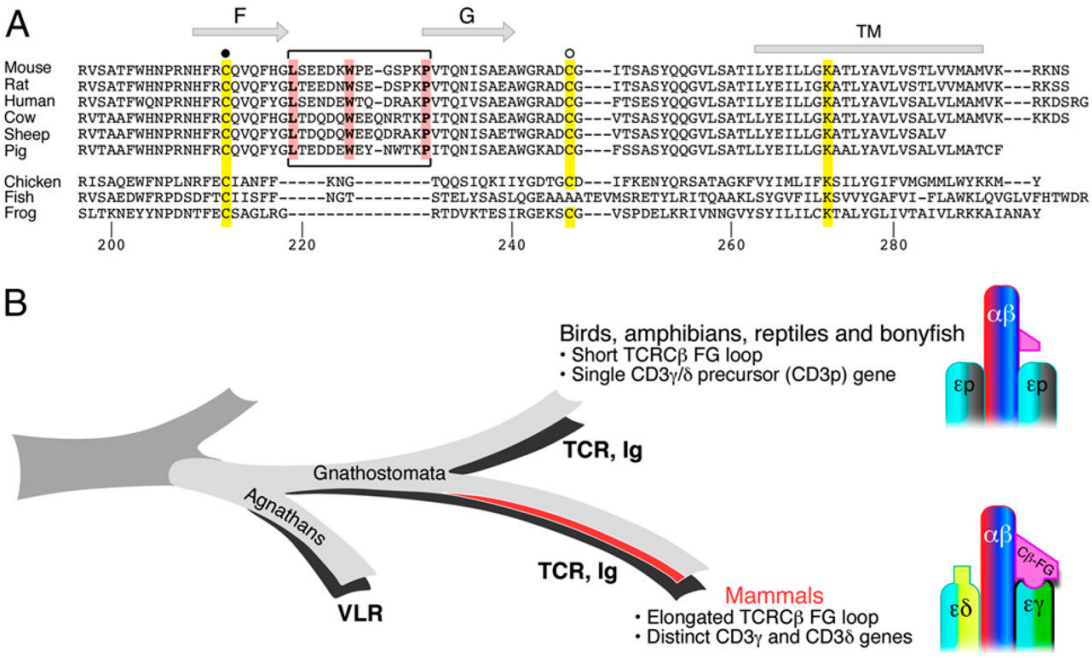

FIGURE 4.

Coevolution of the elongated TCRCβ FG loop and CD3γ plus CD3δ genes from a single precursor in Gnathostamata, a group of vertebrates with adaptive immunity involving a recombinatorial system (VDJ). *A*, Sequence comparison of the TCRCβ FG loop regions among various species. The position of the F- and G-strands is defined based on the N15 TCR structure (16). The bracket region defines the elongated FG loop in mammalian species with well-conserved key residues (L219, W225, and P232) forming the hydrophobic core. The two cysteines contributing to the intrachain and an interchain disulfide bond are indicated by ● and ○, respectively. The conserved lysine residue in the transmembrane region of Cβ is also highlighted in yellow. *B*, Schematic representation of evolutionary relationships between TCRβ and CD3 gene products. Possession of adaptive immunity with recombinatorial-based immune receptors is known for agnathans and gnathostomates. Gnathostomates possess a developed adaptive immune system supporting various VDJ recombinations for Ig and TCR rearrangement, whereas Agnathans do not but contain variable lymphocyte receptors. Distinctions among features of mammals and those of birds, amphibians, reptiles, and bony fish are described and shown schematically.

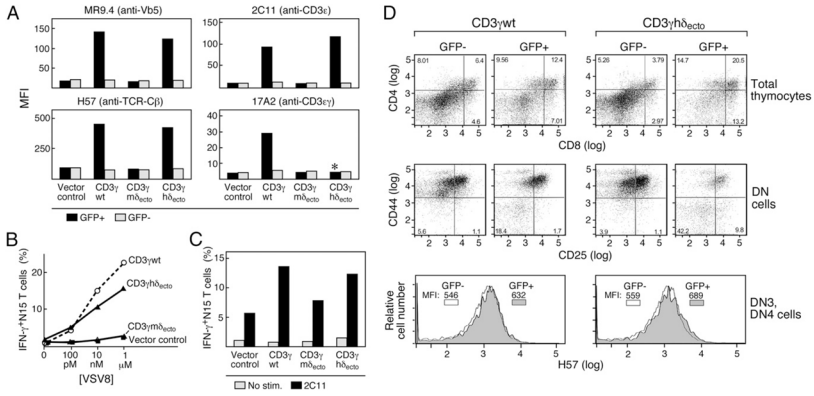

FIGURE 5.

Restoration of T cell signaling by replacing the ectodomain of mCD3γ with that of hCD3δ, but not mCD3δ. *A*, Surface TCR expression on N15TCRtgCD3γ$^{-/-}$T cells resulting from chimeric CD3γ transduction. N15 T cells were stained with the indicated anti-TCR mAb for flow cytometric analysis after retroviral transduction with results of one of three representative experiments shown. *B*, pMHC/TCR-mediated signaling in N15 T cells. Transduced N15TCRtgCD3γ$^{-/-}$T cells were stimulated with VSV8 peptide-loaded APCs for 4 h. The number of cytokine-producing cells was measured using flow cytometry after gating GFP^{+}CD8^{+} populations. *C*, Anti-CD3ε mAb stimulation. Transduced N15 T cells were stimulated by plate-bound 2C11 Ab (5 μg/ml) for 3 h. GFP^{+} CD8^{+} populations were gated for IFN-γ^{+} analysis. *D*, Thymocyte development in CD3γ$^{-/-}$ FTOC by retroviral transduction of CD3γhδ$_{ecto}$ or CD3γwt cDNAs. The transduced (GFP^{+}) and nontransduced (GFP^{-}) cells were separately analyzed. The percentages of cells in the CD4SP, CD8SP, and DP quadrants are shown in the *top panels*. The percentages of cells in theDN3 (CD44^{-}CD25^{+}) and DN4 (CD44^{-}CD25^{-}) quadrants are shown in the middle panels after DN population(CD4^{-}CD8^{-}) gating. Histograms on the *bottom panels* show H57 staining for DN3 and DN4 subpopulations combined (CD4^{-}CD8^{-}CD44^{-}).

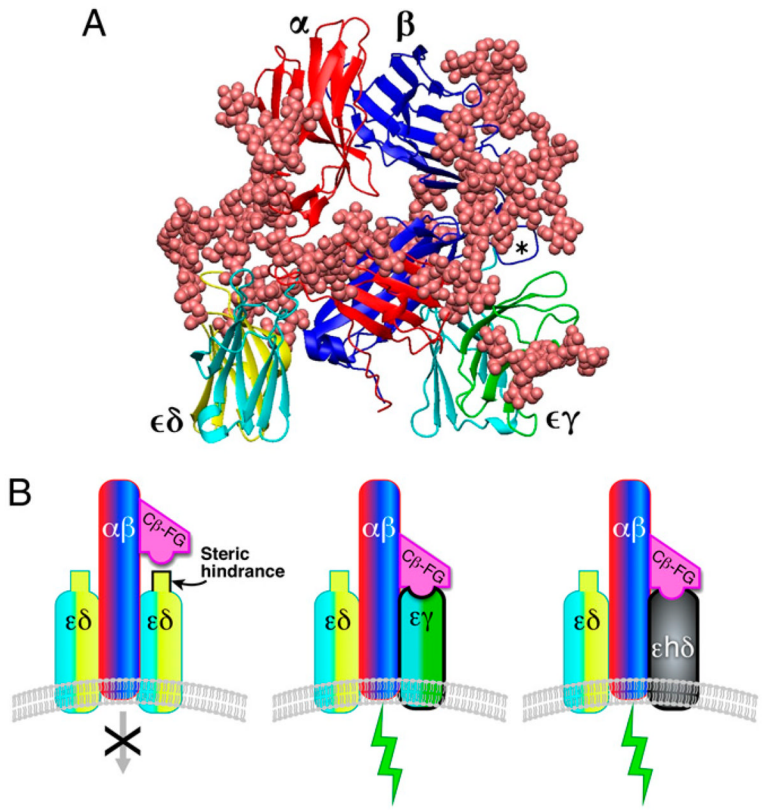

FIGURE 6.

The αβTCR quaternary complex and T cell signaling. *A*, αβ TCR quaternary structure model. This model includes αβ (red/blue), CD3εγ (cyan/green), and CD3εδ (cyan/yellow) heterodimers. The high-mannose *N*-glycans [-(*N*-acetylglucosamine)$_2$-(mannose)$_7$] shown in brown are taken from models solved by Wyss et al. (49). The protruding Cβ FG loop is denoted by an asterisk and overrides the top of the CD3εγ ectodomain, as shown in the figure and Supplemental Fig. 2. *B*, Schematic representations of TCR assembly and signaling involving the TCRβ–CD3εγ module. The models show that an intact TCRβ–CD3εγ module geometry is required for both TCR surface expression and signaling. Steric clash prevents the Cβ FG loop juxtaposition with mCD3εδ, but not mCD3εγ or the interspecies mCD3ε/hCD3δ heterodimer. For simplicity, CD3ζ and the Cyt tail regions of the depicted CD3 subunits are not visualized.